Original Papers

Structural Analysis of High-Silica Ferrierite with Different Structure-Directing Agents by Solid-State NMR and *Ab Initio* Calculations

Hideyuki OKA*† **and Hiroshi OHKI****

*Analysis & Research, TOSOH Analysis and Research Center, Shunan, Yamaguchi 746–0006, Japan
**Department of Chemistry, Faculty of Science, Shinshu University, Asahi, Matsumoto 390–8621, Japan

The host-guest interaction in high-silica ferrierite (FER) with different structure-directing agents (SDA), pyridine and piperidine, was analyzed by solid-state ^{29}Si NMR relaxation experiments and molecular-orbital calculations. Qualitative and quantitative knowledge of the SDA structure obtained by these methods provides significant insight for understanding the functions in a template, and the stabilizing role of the SDA. Relaxation experiments show a larger magnetic dipolar interaction between the silicon and hydrogen atoms in piperidine as compared to that in pyridine, and the results correlate with the bonding property in terms of the distance between the zeolite framework and the SDA. The ^{1}H MAS NMR spectrum shows that the pyridine molecules mainly act as pore fillers in the pyridine-FER. In contrast, it was presumed that piperidine, adjacent to the aluminosilicate framework and framework defects, acted as a counter cation to balance the charge in the piperidine-FER. H^{+}-FER synthesized with piperidine shows a lower hydrothermal stability as compared to that synthesized with pyridine. The hydrothermal stability of H^{+}-FER is discussed by considering the contributions of framework defects and the different properties pertaining to the bonding between the zeolite framework and the SDA.

Introduction

Zeolite ferrierite (FER) is crystalline aluminosilicate that has silicon 5-, 6-, 8-, and 10-membered rings (MR) (Fig. 1).[1,2] The pore sizes of the aluminum-containing FER framework with free diameters of $d \leq 0.48$ nm (8-MR) and $d \leq 0.54$ nm (10-MR).[1,3] The main channel is outlined by elliptical 10-MR, while the side channel is formed by 8-MR. It is possible to synthesize low-silica FER without a structure-directing agents (SDA), while the addition of an SDA is essential for the successful synthesis of high-silica (Si/Al ratio >5) FER.

Owing to its strong hydrophobicity and high thermal stability, high-silica FER is considered to be a light hydrocarbon absorbent and catalyst material.[4,5]

On the other hand, it has been reported that the hydrophobicity and hydrothermal stability of H^{+}-FER differ, depending on the type of SDA used, and only H^{+}-FER crystallized by using pyridine shows high hydrophobicity and structural stability.[6]

To clarify the properties of H^{+}-FER, it is necessary to understand the structure of as-synthesized zeolites, that is, it is essential to understand the functions in a template and the stabilizing role of the SDA.

Using techniques such as XRD, NMR, Raman experiments, and a computational study, the location of an interaction between organic molecules and the FER zeolite frameworks has been investigated to obtain information on their functions in a template.[7-13]

Solid-state NMR studies have been conducted to obtain structural information on zeolites containing organic SDA molecules. ^{29}Si cross-polarization/magic angle spinning (CP/MAS) NMR spectroscopy has been applied to characterize the interaction between the SDA and silicate in a synthesis system of high-silica ZSM-5 zeolite.[14] In as-synthesized aluminosilicate MCM-41 and silicate materials, two-dimensional (2D) solid-state NMR measurements using a heteronuclear magnetic dipolar interaction[15,16] are useful for determining the
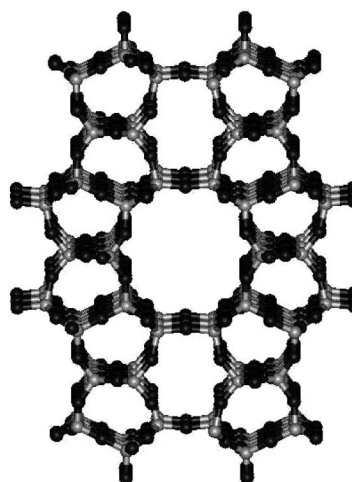

Fig. 1 Ferrierite structure: 10-MR main channels view down the [001] direction.

---

† To whom correspondence should be addressed.
E-mail: oka@tosoh-arc.co.jp

bonding property of the SDA.[17,18]

Solid-state NMR can be used to obtain structural information on various solid materials without any treatment. Since these spectra are sensitive to the local structure of the sample, solid-state NMR is well suited for investigating the local structure of a particular zeolite with an SDA. However, few investigations have been attempted to obtain significant insight on the functions in a template, so as to understand the stabilizing role of the SDA in FER zeolite, and to clarify the different properties of H$^+$-FER, depending on the type of SDA used.

In this study, we conducted solid-state NMR analysis and molecular orbital calculations on high-silica FER with different SDAs, pyridine, and piperidine, and have quantitatively analyzed the SDA that interacts with aluminosilicate.

Experimental

Samples

High-silica FER with an SDA was synthesized under hydrothermal conditions from a reaction mixture containing amorphous silica, $NaAlO_2$, NaOH, water, and one of two types of SDA (pyridine and piperidine).[6] After calcination at 973 K for removal of the SDA, the remaining Na$^+$ ions were exchanged with NH$_4$$^+$ ions, and H$^+$-FER was obtained by the calcination of NH$_4$-FER at 773 K.

The sample composition was analyzed by inductively coupled plasma atomic emission spectroscopy (ICP-AES) and elemental analysis of C, H, and N. The chemical formulas of high-silica FER with SDA were $Na_{1.1}Si_{35}Al_{1.1}O_{72}(C_5H_5N)_{3.0}$ for pyridine-FER and $Na_{0.3}Si_{35}Al_{1.1}O_{72}(C_5H_{11}N)_{3.8}$ for piperidine-FER. The Si/Al ratios were 32 for both pyridine-FER and piperidine-FER. The Na/Al ratios were 1.0 for pyridine-FER and 0.26 for piperidine-FER.

Solid-state NMR

Zeolite samples with different SDAs were dehydrated for 24 h at room temperature below 0.13 Pa (10^{-3} Torr). The dehydrated samples were then packed into NMR rotors with 4.0 and 5.0 mm diameter in a N_2 glove box for analysis.

Solid-state NMR measurements were performed on Varian VXR-300S and Varian NMR Systems 400 multinuclear spectrometers in magnetic fields of 7.1 and 9.4 T, respectively. ^{1}H (399.8 MHz) MAS NMR spectra of SDA-containing FER and H$^+$-FER were obtained using a π/2 pulse of 2.1 μs and a delay time of 10 s between single pulses at sample spinning rates of 15 and 10 kHz, respectively. H$^+$-FER samples were packed under a dry N_2 atmosphere into gas-tight MAS rotors and spun in N_2 gas. ^{29}Si (59.6 MHz) MAS NMR was measured with a π/6 pulse of 1.5 μs and a delay time of 10 s between single pulses at a sample spinning rate of 4 kHz. ^{13}C (100.6 MHz) and ^{29}Si (59.6 MHz) CP/MAS experiments were performed under the Hartmann–Hahn condition; the pulse length was π/2 (2.2 μs for ^{13}C and 4.5 μs for ^{29}Si), which was followed by a contact time of 2.0 and 2.5 ms using a tangent ramp on ^{1}H[19] for ^{13}C with a spinning rate of 10 and 4 kHz, respectively. The radio-frequency field amplitude corresponds to 50 kHz for the ^{1}H and ^{29}Si CP pulses. The NMR chemical shifts for ^{1}H, ^{13}C and ^{29}Si were referenced to external TMS. In all cases it was checked that there was a sufficient delay between the scans allowing a full relaxation of the nuclei.

^{29}Si NMR relaxation measurements of $T_1{}^{HSi}$ were obtained by performing CP experiments with variable contact time pulses ranging from 100 μs to 10 ms. The expression given in Eq. (1) was used to fit the CP peak intensity curves. Here, $M(t)$ is the peak intensity as a function of the contact time, t; $T_{1\rho}{}^H$, the proton spin-lattice relaxation time in the rotating frame; and $T_1{}^{HSi}$, the cross-polarization time constant.[20,21]

$$M(t) = \frac{M_0}{1-\lambda}\left\{\exp\left(\frac{-t}{T_{1\rho}{}^H}\right) - \exp\left(\frac{-t}{T_1{}^{HSi}}\right)\right\}$$

$$\lambda = T_1{}^{HSi}/T_{1\rho}{}^H \qquad\qquad (1)$$

FT-IR

FT-IR microscope spectra were obtained using a Perkin-Elmer Spectrum 2000 spectrometer at a resolution of 4 cm^{-1} with 256 scans. IR data were collected using the attenuated total reflectance (ATR) technique with a single-bounce Ge crystal. IR samples were prepared as powder.

Molecular orbital calculation

The *ab initio* molecular orbital calculations were performed with the Gaussian 03W program[22] using B3LYP/6-31G*. The model structures of the SDA-containing FER were build based on the adjacent binding site with the 10-MR main channel. For the cluster model of aluminosilicate, the silicon atom at site T2 in the 10-MR[23] replaces the aluminum atom. The SDA molecule was imposed into the possible binding sites as a starting conformer.

Hydrothermal stability test

The BET surface area was measured to test the hydrothermal stability of H$^+$-FER. To perform an accelerated hydrolysis stability test, the samples were treated at 1273 K for 5 h in air containing 10% steam. Nitrogen adsorption isotherms were collected on a Belsorp 28SA instrument at 77 K.

Results and Discussion

Solid-state NMR

First, the SDA in the as-synthesized FER was analyzed by solid-state NMR experiments. Figure 2 shows the ^{13}C CP/MAS and ^{1}H MAS NMR spectra for the FER synthesized with pyridine and piperidine as the SDA.

The ^{13}C CP/MAS NMR spectrum for the pyridine-FER shows that the peaks at 151, 135 – 138, and 123 – 126 ppm correspond to the methine groups at the 2 and 6 positions, 4-position, and 3 and 5 positions for pyridine, respectively.

The splitting of the carbon peaks is in good agreement with the result of two crystallographically different pyridine molecules in the pyridine-FER by single-crystal X-ray diffraction.[9]

^{13}C peaks for the piperidine-FER at 23.2 and 45.6 ppm correspond to the carbon species of the methylene groups at the 3, 4, and 5 positions, and at the 2 and 6 positions for piperidine, respectively, although we observed frequency shifts slightly higher than the reported values of 25.2, 27.2 and 47.5 ppm for piperidine molecules in CDCl$_3$.[24]

The ^{1}H MAS NMR spectrum for the pyridine-FER suggests that the ^{1}H peaks at 7.2, 7.5, and 8.5 ppm can be attributed to the proton species of the methine groups at the 3 and 5 positions, 4-position, and 2 and 6 positions for pyridine, respectively.[9] No pyridine comprises hydrogen bonded with silanol, which is observed at ~10 ppm,[25] and the Na/Al ratio of 1.0 suggest that the pyridine molecules mainly act as pore fillers in the zeolite, and do not act as counter cations to balance the charge with the zeolite framework.

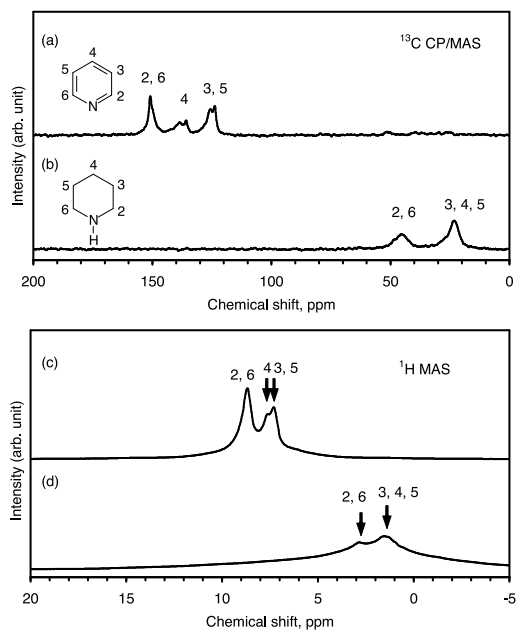On the other hand, the ^{1}H peaks of the piperidine-FER are

Fig. 2 ^{13}C CP/MAS and ^{1}H MAS NMR spectra of high-silica FER synthesized with different SDAs: (a, c) pyridine-FER and (b, d) piperidine-FER.
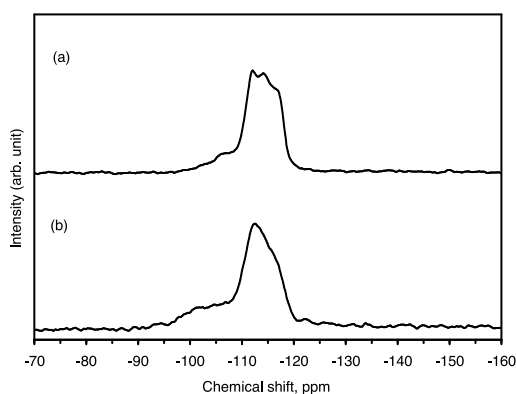

Fig. 3 ^{29}Si MAS NMR spectra of high-silica FER synthesized with different SDAs: (a) pyridine-FER and (b) piperidine-FER.
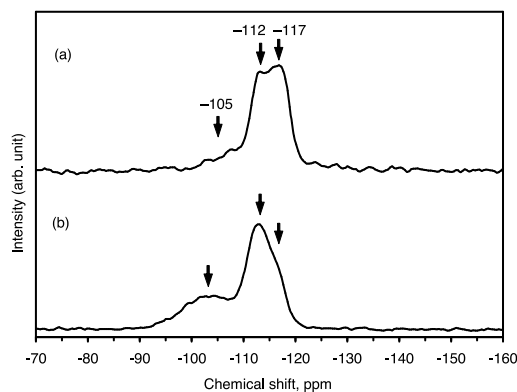

Fig. 4 ^{29}Si CP/MAS NMR spectra of high-silica FER synthesized with different SDAs: (a) pyridine-FER and (b) piperidine-FER.
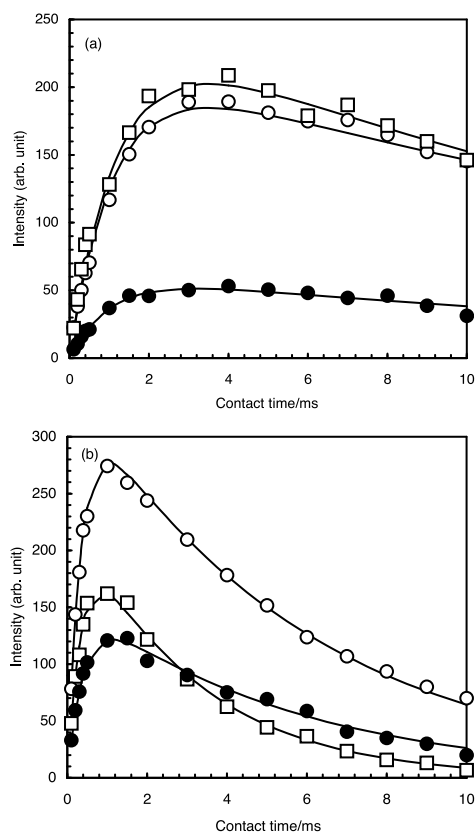

Fig. 5   Variation of the ^{29}Si CP/MAS intensities of the Q^4 and Q^3 signals of high-silica FER synthesized with different SDAs as a function of the contact time: (a) pyridine-FER (● Q^4(1Al); ○ $Q^4{}_1$; □ $Q^4{}_2$) and (b) piperidine-FER (● Q^3; ○ $Q^4{}_1$; □ $Q^4{}_2$).

broader than those of the pyridine-FER, and are inferior with regard to the line intensity. The ^{1}H peaks at 1.5 and 2.8 ppm are assigned to the methylene groups at the 3, 4, and 5 positions, and at the 2 and 6 positions for piperidine, respectively.[24] The broadened ^{1}H resonances show large magnetic dipolar interactions, which is probably due to the different dipole-dipole coupling distances between protons in pyridine and piperidine molecules.

The ^{29}Si MAS NMR spectra of the FER synthesized with pyridine and piperidine are shown in Fig. 3.   The peak at −105 ppm of the pyridine-FER is assigned to Q^4(1Al) sites, giving an Si/Al ratio equal to 35, which is in reasonable agreement with the Si/Al = 32 from a chemical analysis. In the piperidine-FER, the Si/Al ratio of 19 is different from the bulk Si/Al ratio of 32, and an enhancement in the intensity of the CP peak at −105 ppm was observed (Fig. 4), which suggests that a high concentration of the silanol groups (Q^3 sites) exists in the piperidine-FER. Thus, the peak at −105 ppm is assigned to Q^3

sites. It should be noted that silanol groups at framework defects may easily form through synthesis of the piperidine-FER. The peaks in the range −112 to −117 ppm are assigned to Q^4 species.   The splitting of the Q^4 peak indicates structurally nonequivalent silicon atoms in the pyridine-FER and piperidine-FER.

Next, relaxation studies of $T_1{}^{HSi}$ measurements were performed to obtain structural information on the bonding property of the SDA in zeolite. Figures 4 and 5 show the ^{29}Si CP/MAS NMR spectra and the CP relaxation curves for the FER synthesized

Table 1   Summary of cross polarization relaxation results of high-silica FER synthesized with different SDAs

	Pyridine-FER			Piperidine-FER		
	$Q^4(1Al)$	Q^4_1	Q^4_2	Q^3	Q^4_1	Q^4_2
T_1^{HSi}/ms	1.02	1.10	1.20	0.36	0.35	0.41
$T_{1\rho}^H$/ms	20.0	23.0	18.7	3.0	5.9	5.5

Fig. 6   FT-IR spectra of high-silica FER synthesized with different SDAs: (a) pyridine and (b) piperidine.

with pyridine and piperidine.

In Fig. 4, the peaks at −105 ppm are assigned to $Q^4(1Al)$ for pyridine-FER and Q^3 for piperidine-FER from the above results. The peaks at −112 and −117 ppm correspond to two Q^4 species (Q^4_1 and Q^4_2), respectively. The split into two peaks of Q^4 may be because at least two inequivalent Q^4 sites exist in the SDA-containing FER. The Q^4_2 peak of piperidine-FER shows a lower intensity as compared to pyridine-FER. Since the ^{29}Si MAS NMR profiles follow the same trend with the lower intensity of Q^4_2 for piperidine-FER, this is because of the difference in the structures of the Q^4 species by the SDA molecules, and is not due to the different efficiency of ^{1}H-^{29}Si polarization transfer.

The results of relaxation studies are summarized in Table 1. The $T_{1\rho}^H$ values of the Q^3 and Q^4 peaks in the piperidine-FER are lower than those of the pyridine-FER (approximately 1/7 – 1/3).

This suggests the difference in the magnitude of the dipole-dipole interaction between protons in the pyridine-FER and piperidine-FER. Using the shortest distance (d) between hydrogen atoms of piperidine and pyridine, the sixth power of the ratio, $(d_{piperidine}/d_{pyridine})^6$, was calculated to be about 1/8. This can almost be explained by the ratio of $T_{1\rho}^H$ in the NMR measurements and the linewidth of the ^{1}H MAS NMR spectra, which suggests that the ^{1}H peaks of the piperidine-FER are broader than those of the pyridine-FER.

T_1^{HSi} is in inverse proportion to the second moment of the dipolar interaction between protons and silicon atoms (M_2^{HSi}).[26] The T_1^{HSi} values of the Q^3 and Q^4 peaks in the piperidine-FER are lower than those of the pyridine-FER (approximately 1/3). If the Hartmann–Hahn condition is satisfied and the velocity of molecular motions does not have a significant difference between the SDAs pyridine and piperidine, the ratio of T_1^{HSi}, ~3 between pyridine-FER and piperidine-FER, indicates that of M_2^{HSi} ($M_2^{HSi}_{piperidine}/M_2^{HSi}_{pyridine}$), and may be related to the difference of the average H-to-Si interatomic distance ($d_{pyridine}/d_{piperidine} = 3^{1/6} – 1.2$). Thus, it appears that the observed T_1^{HSi} arises from the average distance between the silicon and hydrogen atoms, and suggests that piperidine is adjacent to the zeolite framework at a distance of about 20% that of pyridine.

Molecular orbital calculation

In order to properly understand the details of the factor that contributed to the interactions, we calculated the zeolite model structures with an SDA by *ab initio* method.

The calculated cluster models were constructed based on the experimental results. As mentioned above, it was presumed that pyridine molecules mainly act as pore fillers in the zeolite, indicating the interaction of pyridine with the silicate structure. The Na/Al ratio of piperidine-FER is 0.26, which significantly differs from the value of 1.0 for pyridine-FER. In addition, the FT-IR spectrum (Fig. 6) of piperidine-FER suggests that the stretching mode of the NH_2^+ group appears as a weak band at 3250 cm^{-1}.[27] This is because the piperidine acts as a counter
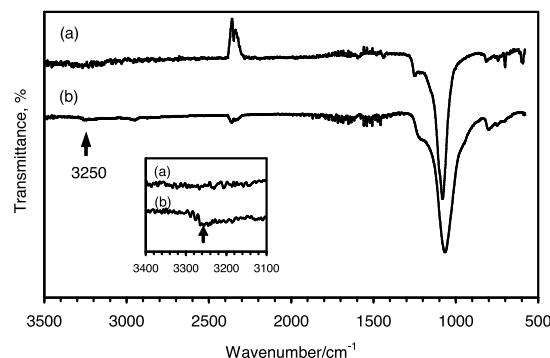
cation to balance the charge with the aluminosilicate framework and/or silanol groups at framework defects that are suggested by the larger Q^3/Q^4 ratio of 0.27 for piperidine-FER than 0.13 for pyridine-FER in the ^{29}Si MAS NMR spectra.

Figures 7 and 8 show the obtained stable structures of the models and the estimated reaction energy, ΔE, between the SDA and zeolite framework. Pyridine reacted with the silicate structure and stabilized at −13.9 kcal mol^{-1}. On the other hand, piperidine in the form of piperidium ions greatly stabilized at −239 kcal mol^{-1}. Further, after reacting with the aluminosilicate and the defects of the silicate structure, piperidine stabilized at −98 and −107 kcal mol^{-1}, respectively. The calculated cluster models indicate that piperidine ions are adjacent to the framework and the hydrogen-bonded complex is formed by framework defects, features consistent with the fact that the cation interacts strongly with the framework.

Thus, it was presumed that pyridine mainly acted as a pore filler, whereas piperidine, which was adjacent to the aluminosilicate framework and framework defects, acted as a counter cation to balance the charge. It can be found that piperidine molecules are closer to the zeolite framework than pyridine molecules.

The average distance between the silicon and hydrogen atoms were 3.4 Å (pyridine-FER) and 2.9 Å (piperidine-FER), and piperidine adjacent to the zeolite framework in a distance of about 16% compared to pyridine. This observation is consistent with the proposed result of T_1^{HSi} in the NMR, which suggests that the average internuclear distance between two atoms is shorter by about 20% in the piperidine-FER than pyridine-FER.

Therefore, it was clarified that the magnitude of dipolar interaction between protons associated with the SDA and the neighboring ^{29}Si nuclei was significantly influenced by the distance between the two atoms. This can be suggested as the reason for the difference in the properties of the bonding between the SDA and the zeolite framework in the pyridine-FER and piperidine-FER; in piperidine, the bonding strongly binds the piperidine molecules coordinated to the aluminum atoms and the framework defect sites.

Hydrothermal stability of H$^+$-FER

From the above-mentioned examination, the high-silica FER with an SDA was studied. Finally, we examined the hydrothermal stability of H$^+$-FER synthesized with different SDAs, pyridine and piperidine.

Figure 9 shows the ^{1}H MAS NMR spectra of the H$^+$-FER zeolites of H-pyridine-FER and H-piperidine-FER. The observed peaks at 1.8, 2.4, and 4.3 ppm are attributed to the
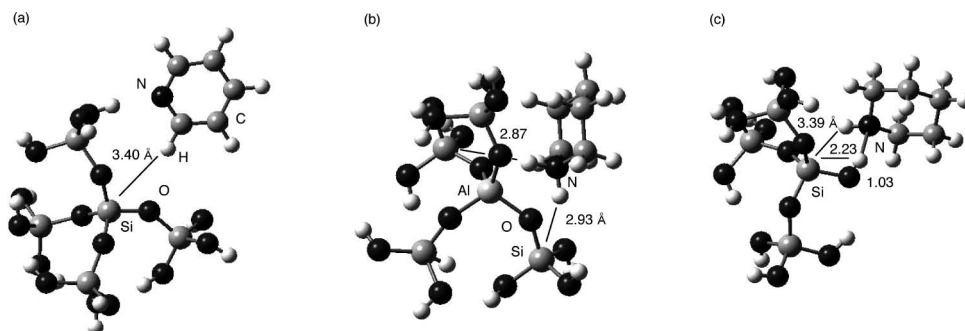
Fig. 7 Optimized cluster models of high-silica FER that interacts with different SDAs: (a) pyridine-FER, (b) [Al-O]⁻-piperidium cation and (c) [Si-O⁻]-piperidium cation.
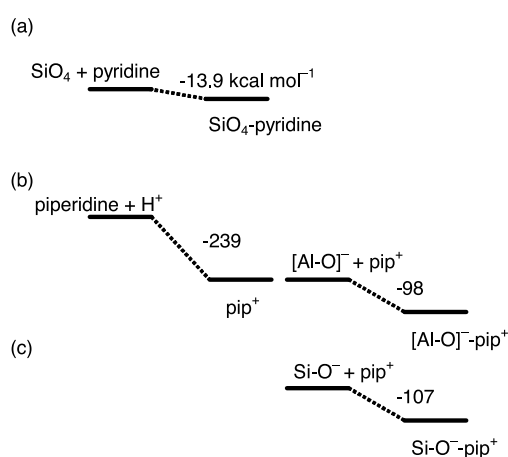

Fig. 8 Estimated reaction energy, ΔE, between the SDA and zeolite framework obtained using *ab initio* calculations: (a) SiO$_4$-pyridine, (b) [Al-O]⁻-piperidium cation (pip$^+$) and (c) [Si-O⁻]-pip$^+$.

Fig. 9 ^{1}H MAS NMR spectra of dehydrated H$^+$-FER synthesized with different SDAs: (a) H-pyridine-FER and (b) H-piperidine-FER. The zeolite samples were dehydrated at an elevated rate of 0.25 K min^{-1} from room temperature to 623 K below 0.13 Pa (10^{-3} Torr) and were held at this temperature for 5 h.

silanol, octahedral aluminum, and Brönsted acid species, respectively.[25,28] This confirms that the ^{27}Al MAS NMR spectra (not shown) indicate the greater presence of octahedral aluminum at 0 ppm in the H-piperidine-FER.

The Brönsted acid species observed for H-pyridine-FER lost intensity in the spectrum of H-piperidine-FER, and the ^{1}H peak of the silanol associated with the imperfections of the zeolite was superior with regard to the line intensity for H-piperidine-FER, with an H-piperidine-FER/H-pyridine-FER ratio of 2.5. In addition, ^{29}Si MAS NMR (not shown) suggests that the Q^3/Q^4 ratio of 0.15 for H-piperidine-FER is larger than that of 0.11 for H-pyridine-FER, indicating the presence of a greater number of framework defects in H-piperidine-FER as compared to H-pyridine-FER. The BET surface areas are 290 m^2 g^{-1} for both non-calcined H$^+$-FER synthesized with pyridine and piperidine. After calcining H$^+$-FER at 1273 K, the surface areas are 292 m^2 g^{-1} for H-pyridine-FER and 250 m^2 g^{-1} for H-piperidine-FER, respectively. H-piperidine-FER shows a small surface area after being calcined at 1273 K, which may be related to the structural change of the zeolite framework. It is found that H-piperidine-FER has a lower hydrothermal stability as compared to H-pyridine-FER, and that the silanol groups at framework defects influence the hydrothermal stability of H$^+$-FER.

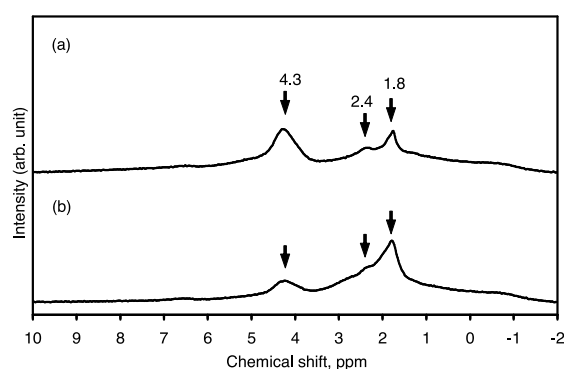As mentioned above, the SDAs in the as-synthesized pyridine-FER and piperidine-FER have different functions in a template and different stabilizing roles. The structural defects may easily form in the piperidine-FER through the synthesis of the FER. It is presumed that the piperidine molecule will be protonated during the synthesis, and interacts strongly with the aluminosilicate framework, and the framework defects acted as a counter cation.

Conclusions

We have conducted solid-state NMR on high-silica FER with different SDAs, pyridine and piperidine. By using this method, we can extract quantitative information about the structure of as-synthesized zeolites.

Based on the obtained data, we concluded that differences arose in the bonding properties based on the distance between the SDA and the zeolite framework. The magnetic dipolar interaction between the silicon and hydrogen atoms is larger in piperidine than in pyridine. The large dipolar interaction observed in the piperidine-FER is caused by the short distance between the silicon and hydrogen atoms in piperidine. While pyridine mainly acts as a pore filler in FER, piperidine, which is adjacent to the aluminosilicate framework and framework defects, acts as a counter cation to balance the charge.

The H$^+$-FER synthesized with piperidine shows low hydrothermal stability as compared to that synthesized with pyridine. This can be explained as being a result of the

formation of framework defects during the synthesis of the FER with piperidine.

References

1. P. A. Vaughan, *Acta Crystallogr.*, **1966**, *21*, 983.
2. I. J. Pickering, P. J. Maddox, J. M. Thomas, and A. K. Cheetham, *J. Catal.*, **1989**, *119*, 261.
3. W. M. Meier and D. H. Olson, "*Atlas of Zeolite Structure Types*", **1992**, Butterworth-Heinemann, Boston.
4. I. D. Harrison, H. F. Leach, and D. A. Whan, *Zeolites*, **1987**, *7*, 21.
5. P. Mériaudeau, C. Naccache, H. N. Le, T. A. Vu, and G. Szabo, *J. Mol. Catal. A*, **1997**, *123*, L1.
6. M. Hironaka, K. Itabashi, and M. Nakano, 13th International Zeolite Conference, Recent Research Reports, **2001**, 14-R-05.
7. R. E. Morris, S. J. Weigel, N. J. Henson, L. M. Bull, M. T. Janicke, B. F. Chmelka, and A. K. Cheetham, *J. Am. Chem. Soc.*, **1994**, *116*, 11849.
8. S. J. Weigel, J.-C. Gabriel, E. Guttierez Puebla, A. Monge Bravo, N. J. Henson, L. M. Bull, and A. K. Cheetham, *J. Am. Chem. Soc.*, **1996**, *118*, 2427.
9. J. E. Lewis, J. Clemens, C. Freyhardt, and M. E. Davis, *J. Phys. Chem.*, **1996**, *100*, 5039.
10. A. Davidson, S. J. Weigel, L. M. Bull, and A. K. Cheetham, *J. Phys. Chem. B*, **1997**, *101*, 3065.
11. D.-C. Lin, H.-Y. He, W.-Z. Zhou, and Y.-C. Long, *Microporous Mesoporous Mater.*, **2005**, *86*, 152.
12. A. B. Pinar, L. Gomez-Hortiguela, and J. Perez-Pariente, *Chem. Mater.*, **2007**, *19*, 5617.
13. R. Garcia, L. Gomez-Hortiguela, I. Diaz, E. Sastre, and J. Perez-Pariente, *Chem. Mater.*, **2008**, *20*, 1099.
14. S. L. Burkett and M. E. Davis, *J. Phys. Chem.*, **1994**, *98*, 4647.
15. A. J. Vega, *J. Am. Chem. Soc.*, **1988**, *110*, 1049.
16. C. A. Fyfe, Y. Zhang, and P. Aroca, *J. Am. Chem. Soc.*, **1992**, *114*, 3252.
17. M. T. Janicke, C. C. Landry, S. C. Christiansen, D. Kumar, G. D. Stucky, and B. F. Chmelka, *J. Am. Chem. Soc.*, **1998**, *120*, 6940.
18. S. C. Christiansen, D. Zhao, M. T. Janicke, C. C. Landry, G. D. Stucky, and B. F. Chmelka, *J. Am. Chem. Soc.*, **2001**, *123*, 4519.
19. B. H. Meier, *Chem. Phys. Lett.*, **1992**, *188*, 201.
20. G. E. Maciel and D. W. Sindorf, *J. Am. Chem. Soc.*, **1980**, *102*, 7606.
21. D. T. Okamoto, S. L. Cooper, and T. W. Root, *Macromolecules*, **1992**, *25*, 1068.
22. Gaussian 03, Revision C.2, M. J. Frisch, G. W. Trucks, H. B. Schlegel, G. E. Scuseria, M. A. Robb, J. R. Cheeseman, J. A. Montgomery, Jr., T. Vreven, K. N. Kudin, J. C. Burant, J. M. Millam, S. S. Iyengar, J. Tomasi, V. Barone, B. Mennucci, M. Cossi, G. Scalmani, N. Rega, G. A. Petersson, H. Nakatsuji, M. Hada, M. Ehara, K. Toyota, R. Fukuda, J. Hasegawa, M. Ishida, T. Nakajima, Y. Honda, O. Kitao, H. Nakai, M. Klene, X. Li, J. E. Knox, H. P. Hratchian, J. B. Cross, C. Adamo, J. Jaramillo, R. Gomperts, R. E. Stratmann, O. Yazyev, A. J. Austin, R. Cammi, C. Pomelli, J. W. Ochterski, P. Y. Ayala, K. Morokuma, G. A. Voth, P. Salvador, J. J. Dannenberg, V. G. Zakrzewski, S. Dapprich, A. D. Daniels, M. C. Strain, O. Farkas, D. K. Malick, A. D. Rabuck, K. Raghavachari, J. B. Foresman, J. V. Ortiz, Q. Cui, A. G. Baboul, S. Clifford, J. Cioslowski, B. B. Stefanov, G. Liu, A. Liashenko, P. Piskorz, I. Komaromi, R. L. Martin, D. J. Fox, T. Keith, M. A. Al-Laham, C. Y. Peng, A. Nanayakkara, M. Challacombe, P. M. W. Gill, B. Johnson, W. Chen, M. W. Wong, C. Gonzalez, and J. A. Pople, Gaussian, Inc., Pittsburgh, PA, **2003**.
23. S. Bordiga, G. T. Palomino, C. Pazè, and A. Zecchina, *Microporous Mesoporous Mater.*, **2000**, *34*, 67.
24. Spectral Database for Organic Compounds (SDBS) prepared by National Institute of Advanced Industrial Science and Technology (AIST), http://riodb01.ibase.aist. go.jp/sdbs/.
25. P. Diehl, E. Fluck, H. Günther, R. Kosfeld, and J. Seelig, "*Solid-State NMR II*", **1994**, Chap. 2, Springer-Verlag, New York.
26. A. Pines, M. G. Gibby, and J. S. Waugh, *J. Chem. Phys.*, **1973**, *59*, 569.
27. R. Kefi, F. Lefebvre, and C. B. Nasr, *Cryst. Res. Technol.*, **2007**, *42*, 333.
28. M. Hunger, M. W. Anderson, A. Ojo, and H. Pfeifer, *Micropor. Mater.*, **1993**, *1*, 17.